Azimuthal and radial shaping of vortex beams generated in twisted nonlinear photonic crystals

Keren Shemer,[1,*] Noa Voloch-Bloch,[1] Asia Shapira,[1] Ana Libster,[1] Irit Juwiler,[2] and Ady Arie[1]

[1]*Department of Physical Electronics, School of Electrical Engineering, Faculty of Engineering, Tel-Aviv University, Tel-Aviv 69978, Israel*

[2]*Department of Electrical and Electronics Engineering, Sami Shamoon College of Engineering, Ashdod 77245, Israel*

**Corresponding author: shemerkeren@gmail.com*

Received July 8, 2013; revised September 24, 2013; accepted November 14, 2013; posted November 15, 2013 (Doc. ID 193591); published December 13, 2013

We experimentally demonstrate that the orbital angular momentum (OAM) of a second harmonic (SH) beam, generated within twisted nonlinear photonic crystals, depends both on the OAM of the input pump beam and on the quasi-angular momentum of the crystal. In addition, when the pump's radial index is zero, the radial index of the SH beam is equal to that of the nonlinear crystal. Furthermore, by mixing two noncollinear pump beams in this crystal, we generate, in addition to the SH beams, a new "virtual beam" having multiple values of OAM that are determined by the nonlinear process. © 2013 Optical Society of America

OCIS codes: (190.2620) Harmonic generation and mixing; (090.2890) Holographic optical elements; (050.4865) Optical vortices.

http://dx.doi.org/10.1364/OL.38.005470

Light beams carrying orbital angular momentum (OAM) are characterized by helical wavefront structures. These beams have a phase singularity at the center of their optical axis, and are also referred to as optical vortices. Allen *et al.* [1] recognized that light beams with an azimuthal phase dependence of $\exp(il\Phi)$ carry an OAM equivalent to $l\hbar$ per photon, where $\hbar$ is the reduced Planck's constant, Φ is the angular coordinate, and the topological charge l can have any integer value. Optical vortices have attracted considerable interest and have been studied intensively in linear and nonlinear optics [2–8]. They can be utilized in various applications such as optical tweezers for trapping and manipulation of microparticles [9,10] or increasing the capacity and speed of optical communications systems by multiplexing carrier waves with different OAM [11]. In addition, entanglement of OAM states of photons can be used for quantum computation and quantum cryptography [12,13].

Several studies were previously reported on nonlinear optical interactions of beams carrying OAM [14–17]. Until now, only two cases were investigated: beams carrying OAM were used to pump a conventional nonlinear crystal [14], and Gaussian beams lacking OAM were used to pump twisted nonlinear photonic crystals (NPCs) [15]. In the first case, the nonlinear crystals lacked quasi-angular momentum; therefore, the OAM of the second harmonic (SH) beam was determined solely by that of the pump beam. In the second case, the OAM of the SH beam was governed only by the crystal's quasi-angular momentum. However, the general case, in which both the pump and the crystal have OAM, has not been studied until now. In this case, demonstrated here experimentally for the first time to our knowledge, the OAM of the generated beam is determined both by the OAM of the pump beam and by the quasi-angular momentum of the crystal. In addition to the azimuthal intensity dependence, we show that the radial dependence of the generated beam can also be controlled by that of the crystal. Taking advantage of phenomena available only in nonlinear interactions opens new possibilities for engineering various OAM states. For instance, mixing two noncollinear beams in the NPC yields "virtual vortices" [15,18,19] with various OAM that are determined by each of the two incident beams.

An example of light beams carrying OAM are Laguerre–Gaussian (LG_{lp}) modes [2–5], described by the azimuthal index l, the number of intertwined helices, and the radial index p, the number of additional concentric rings. These modes have amplitude distributions at the origin given by

$$U_{l,p}(r,\varphi,0) = U_0\left(\frac{r\sqrt{2}}{\omega_0}\right)^{|l|}\exp\left(-\frac{r^2}{\omega_0^2}\right)L_p^{|l|}\left[\frac{2r^2}{\omega_0^2}\right]\exp(il\varphi), \tag{1}$$

where $L_p^{|l|}$ are the generalized Laguerre polynomials and ω_0 is the radius of the beam waist. When $l \neq 0$, the beam has an appearance of $p+1$ annular rings. When $l = 0$, the modes have a bright central spot surrounded by p concentric rings. When $l = 0$ and $p = 0$, the beam has a simple Gaussian profile.

The generation of nonlinear SH beams carrying OAM was recently studied in [15,16], where twisted NPCs were transversely illuminated with a Gaussian pump beam lacking OAM. The second-order nonlinear susceptibility of these twisted NPCs was represented by various binary modulation functions with a geometrical singularity, e.g., a fork-shaped hologram. In this configuration, the phase matching is partially satisfied through the nonlinear Raman–Nath process [20], yielding a multiorder nonlinear SH diffraction at angles of: $\theta_m = \sin^{-1}(m \cdot \lambda_{2\omega}/\Lambda)$, where m is the diffraction order, $\lambda_{2\omega}$ is the SH wavelength, and Λ is the poling period. The general conservation law for the OAM in this SH generation process [15] is

$$l_{2\omega,m} = 2 \cdot l_\omega + m \cdot l_c, \tag{2}$$

where $l_{2\omega}$ is the OAM of the SH wave, l_ω is the OAM of the pump wave, m is the diffraction order, and l_c is the crystal's quasi-angular momentum.

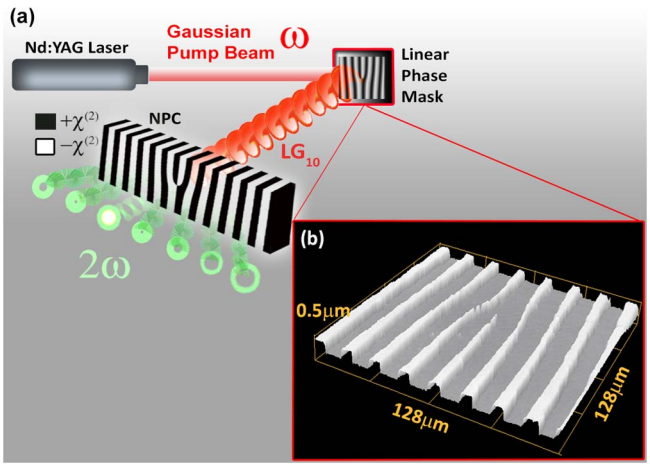

Fig. 1. Experiment Setup. (a) Beams carrying OAM are generated by the use of a fork-shaped linear phase mask. The filtered first diffraction order (LG_{10}) transversely illuminates the twisted NPC, yielding various SH vortices. (b) 3D microscope image of the fabricated linear phase mask.

It can be shown in a similar manner to [15] that, for a pump beam with a radial index of zero, the radial index of the output SH beam is equal to that of the crystal.

In this Letter, we report the first experimental observation of the general OAM conservation law for a nonzero OAM of the pump and crystal. The experimental setup is shown in Fig. 1. A linear phase mask was used to generate a variety of LG modes from a y-polarized Nd:YAG Q-switched laser operating at a wavelength of 1064.5 nm. The axes are defined according to the crystallographic directions in the nonlinear crystal. The reflected first diffraction order was spatially filtered and focused by a lens to a 180 μm waist (ω_0) on the twisted NPC (in the transverse configuration). Spectral filters placed after the NPC filtered the pump's radiation and maintained only the SH radiation. A CCD camera, placed 15 cm after the crystal, captured the focused output vortex beams. The peak power of the incident vortex pump beam was 6.7 kW and the generated SH peak power was 36 μW on average. Using different NPC structures, we studied both the azimuthal and the radial dependence of the crystals on the generated output beams.

These NPC structures were designed based on the concept of binary nonlinear holograms [16]. They were then fabricated by two-dimensional electric field poling of a 0.5 mm thick stoichiometric lithium tantalate nonlinear crystal. The crystal had four separate 0.5 mm × 0.5 mm structures, with different modulations of the second-order nonlinearity coefficient. They were chosen to generate four different LG modes from a fundamental Gaussian mode: LG_{01}, LG_{02}, LG_{20}, and LG_{11}. The modulation frequency in the x direction, f_{carrier}, was 0.035 μm^{-1}. Microscope images compared to the theoretical designs of all the structures are shown in Fig. 2 (the nonlinear modulation is revealed by the selective etching of the crystal surface).

The linear phase mask that was used to shape the fundamental beam was fabricated by a standard e-beam lithography technique. The mask consisted of a 255 nm patterned layer of gold on top of a 70 nm gold film over a 20 nm chromium-coated silicon wafer [21].

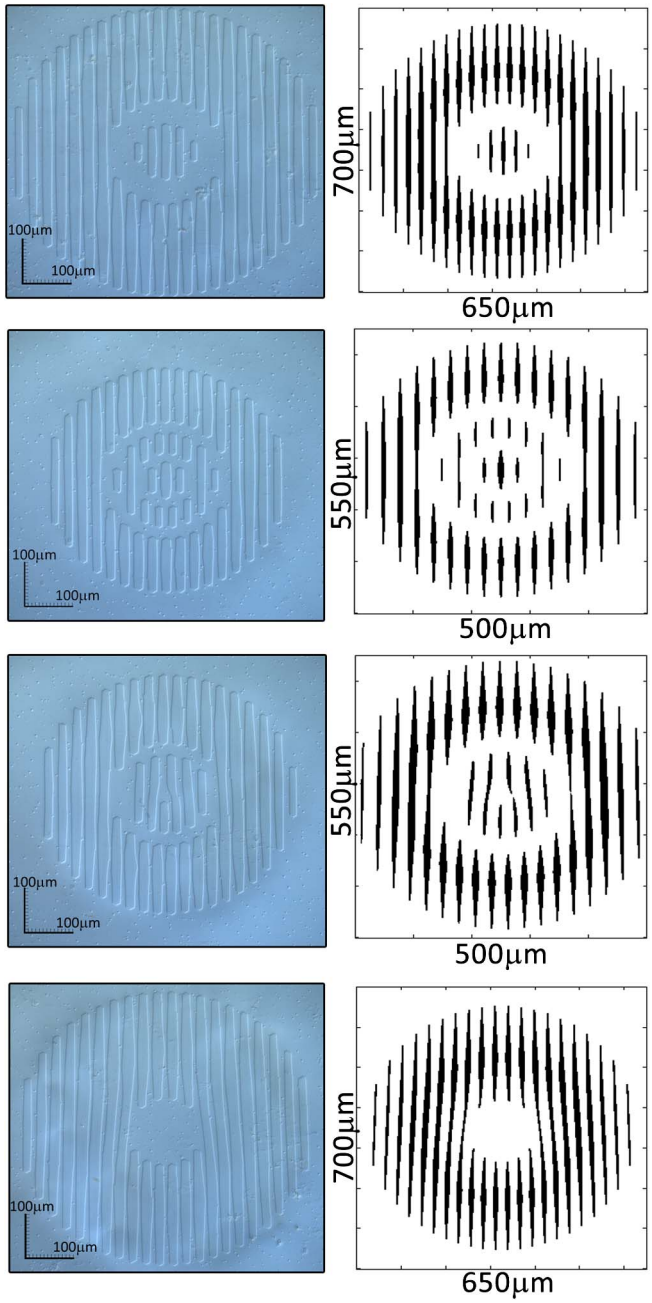

Fig. 2. NPC Structures. Microscope images of the poling patterns of the fabricated NPC structures (left) versus their theoretical designs (right). Top to bottom: LG_{01}, LG_{02}, LG_{11}, and LG_{20}.

The mask had two 0.8 mm × 0.8 mm structures, each with a different LG mode: LG_{10} [shown in Fig. 1(b)] and LG_{20}. The patterned layer's thickness was optimally designed for a 15° reflection angle.

In Figs. 3 and 4, the measured profiles are compared to numerical results, computed by a split-step beam propagation method. The azimuthal dependence is shown in Figs. 3(a) and 3(b) for NPCs with $l_c \neq 0$ and $p_c = 0$, while the radial dependence is shown in Fig. 4 for NPCs with $l_c = 0$ and $p_c \neq 0$. Figure 3(c) combines both cases with $l_c = p_c = 1$.

These results verify the aforementioned OAM conservation law [Eq. (2)]. For each profile in Figs. 3(a)–3(c), one can readily distinguish the orders (framed in dashed

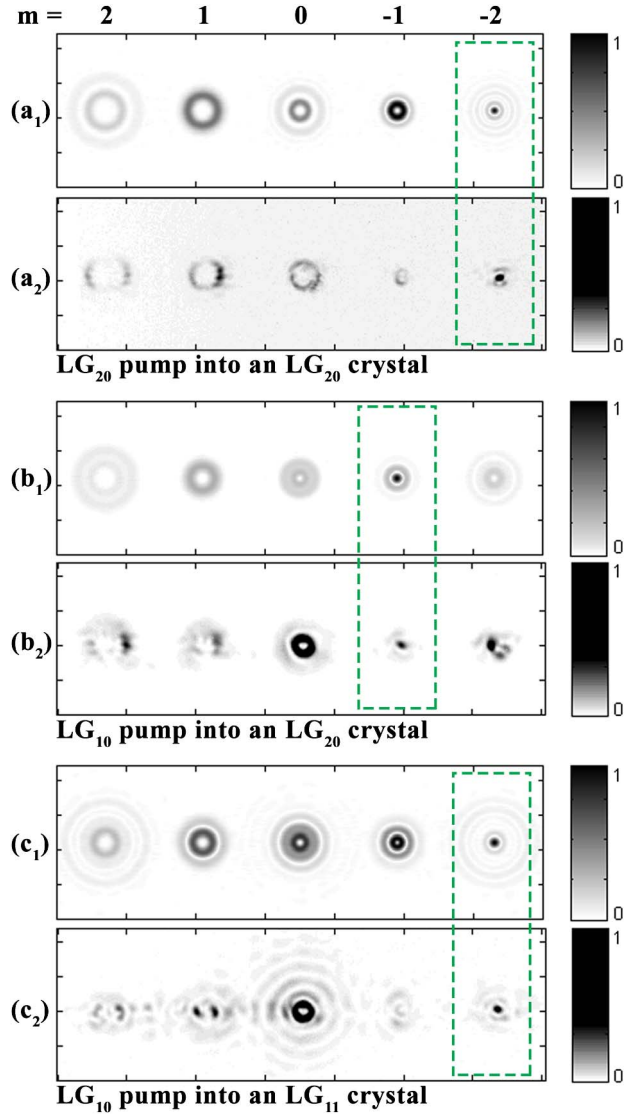

Fig. 3. Azimuthal control. Numerical (subscript 1) compared to experimental (subscript 2) profiles of (a) an LG_{20} fundamental beam entering an LG_{20} NPC, and an LG_{10} fundamental beam entering (b) an LG_{20} NPC and (c) an LG_{11} NPC. The orders where $l_{2\omega} = 0$ are framed by dashed lines. All images are 7 mm wide by 2.2 mm long.

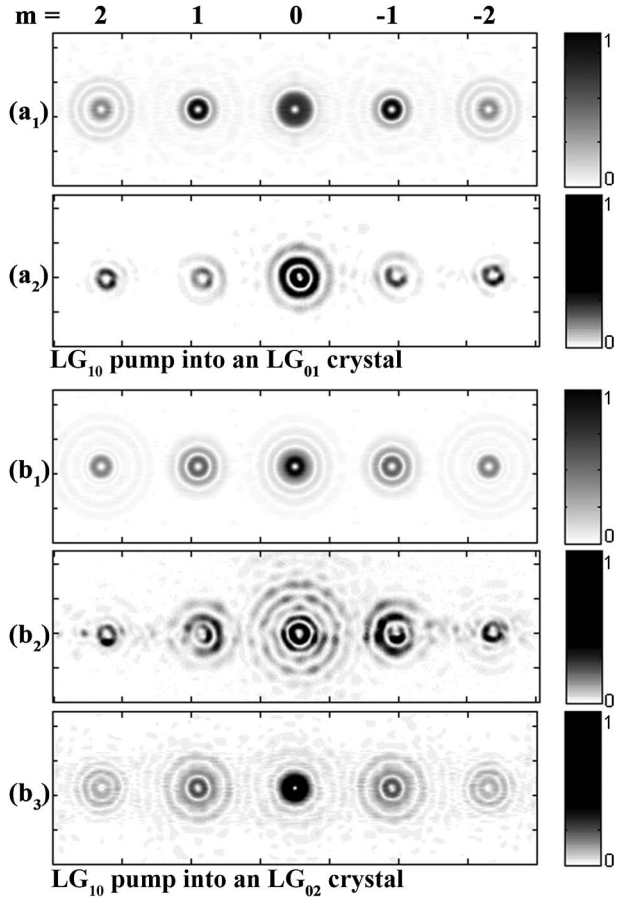

Fig. 4. Radial Control. Numerical (subscript 1) compared to experimental (subscript 2) profiles of an LG_{10} fundamental beam entering (a) an LG_{01} NPC and (b) an LG_{02} NPC. (b_3) Numerical profile after considering the linear phase mask on the crystal's facet. All images are 7 mm wide by 2.2 mm long.

lines) where the OAM vanishes, i.e., a Gaussian mode with $l_{2\omega} = 0$ is observed. As an example, Fig. 3(a) shows that when an LG_{20} input beam enters an LG_{20} structure, a Gaussian mode is observed at the $m = -2$ diffraction order since, in this case, $l_\omega = 2$, $l_c = 2$. The remaining diffraction orders $m = -1$, 0, 1, 2 have an output OAM of $l_{2\omega} = 2$, 4, 6, 8, respectively. Similarly, for an LG_{10} input beam entering an LG_{20} (LG_{11}) structure, a Gaussian mode is observed at order $m = -1$ ($m = -2$), as shown in Figs. 3(b) and 3(c), respectively. The different radii of the vortices in Fig. 3 arise from the different topological charge of the beams in each order, which is governed, per profile, by the product of the crystal's quasi-angular momentum and the diffraction order. For the two cases shown in Fig. 4, $l_c = 0$; hence, all the modes have the same azimuthal dependence and subsequently the same inner radius. However, the nonlinear crystal determines the radial dependence of the generated beams. Specifically, LG_{21} and LG_{22} modes, having 2 and 3 concentric rings, were obtained in the first diffraction order in Figs. 4(a) and 4(b), respectively. In Fig. 5, the combined results from all the experiments of the measured vortices' radii as a function of the topological charge are shown. The radius was measured as the distance from the vortex's (dark) center to the highest intensity ring. The measurements are in good agreement with the vortices' radii obtained from the numerical simulation [for LG_{20} at $l = 6$, the signal was very weak, as can be seen in Fig. 3(b_2), which may explain the larger deviation from the expected numerical value for this beam]. The additional concentric rings observed in some of the experimental profiles result from the linear phase mask on the crystal's facet, originating from the selective etching of the crystal surface [see Fig. 4(b_3) for an example of a simulation profile after taking this into account]. This parasitic effect can be eliminated by polishing the crystal facets. The mode purity of the first five orders of the simulation profile for an LG_{10} beam entering an LG_{20} crystal, with respect to the theoretical LG mode, ranged from 87% to 99%. As can be noticed, some of the weaker outer rings that appear in the simulation are not observed in the experimental profiles, probably due to the relatively weak SH signal.

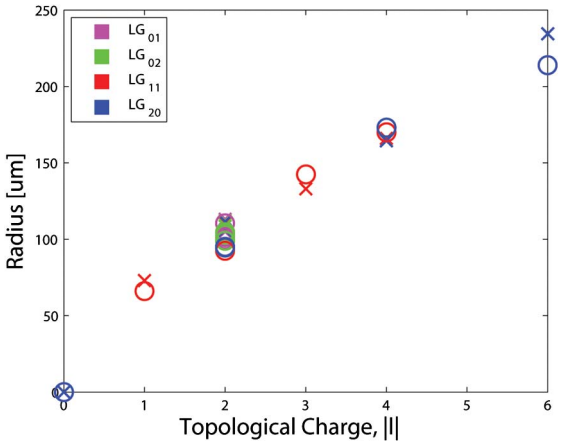

Fig. 5. Vortices' radius. Numerical (circles) and experimental (crosses) results for the SH vortices' radii as a function of the topological charge.

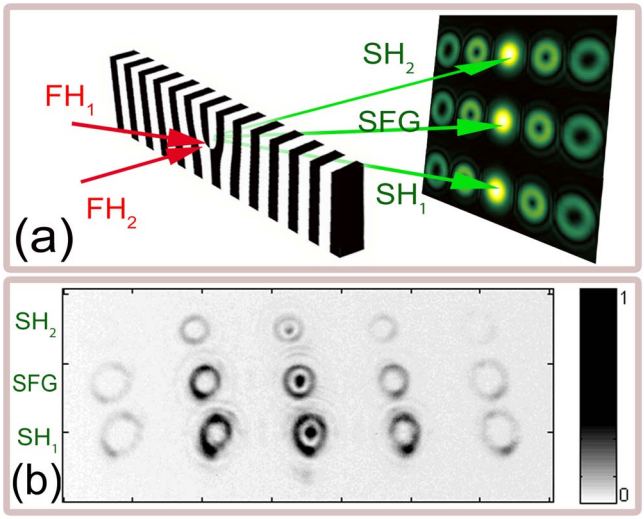

Fig. 6. Generation of virtual vortex beams. (a) Experimental setup: two noncollinear beams interfere inside the twisted NPC. The resulting nonlinear diffraction pattern includes the SH of each of the input beams (top and bottom rows), as well as the SFG from both beams (middle row). (b) Experimental profile captured 7.5 cm after an LG_{20} NPC. The image is 7 mm wide by 3 mm long.

The NPC can also be used to up-convert more than one beam [15]. For this purpose, we constructed the experimental setup shown in Fig. 6(a), where the NPC is illuminated simultaneously by two noncollinear beams. The Gaussian pump beam from the aforementioned laser was divided in two, using mirrors and beam splitters. The two beams, with an angle of 9 mrad between them, were directed to interfere inside the twisted NPC. The captured profile, 7.5 cm after the crystal, is shown in Fig. 6(b). Here the nonlinear diffraction pattern includes the SH of each of the input beams (upper and bottom rows), as well as a new set of vortices generated by the sum-frequency generation (SFG) nonlinear process (middle row). The OAM of the "virtual vortices" is $l_{SFG} = l_1 + l_2 + ml_c$. In this case, since $l_1 = l_2 = 0$, all three profiles (rows) are identical.

Hence, the SFG process mixes not only frequencies but also the value of the angular momentum. These virtual vortices are the outcome of a mutual diffraction process and are a unique nonlinear phenomenon with no analogy in linear optics. Further control of the OAM of the virtual vortices can be achieved by pumping the NPC with beams that carry different OAM and even different frequencies [15]. This enables the generation of multiple vortices having various charges at various diffraction angles.

In conclusion, we studied the general case of input pump beams, carrying OAM, illuminating transversely NPC structures with quasi-angular momentum. These structures have an active role in shaping the output beam's profile. We experimentally confirmed the general OAM conservation law, i.e., the topological charge of the SH beam is shown to be the sum of twice the charge of the input beam and the charge of the NPC. Furthermore, we demonstrated nonlinear optical shaping of the output vortices' radial component. Dual beam control of the generated beam, based on the virtual vortices phenomena, provides an example of the new wide-ranging possibilities for all-optical twisting of light.

References

1. L. Allen, M. W. Beijersbergen, R. J. C. Spreeuw, and J. P. Woerdman, Phys. Rev. A **45**, 8185 (1992).
2. L. Allen, M. J. Padgett, and M. Babiker, Prog. Opt. **39**, 291 (1999).
3. A. M. Yao and M. J. Padgett, Adv. Opt. Photon. **3**, 161 (2011).
4. G. Molina-Terriza, J. P. Torres, and L. Torner, Nat. Phys. **3**, 305 (2007).
5. S. Franke-Arnold, L. Allen, and M. J. Padgett, Laser Photon. Rev. **2**, 299 (2008).
6. I. V. Basistiy, V. Yu. Bazhenov, M. S. Soskin, and M. V. Vasnetsov, Opt. Commun. **103**, 422 (1993).
7. A. S. Desyatnikov, Y. S. Kivshar, and L. Torner, Prog. Opt. **47**, 291 (2005).
8. J. Courtial, K. Dholakia, L. Allen, and M. J. Padgett, Phys. Rev. A **56**, 4193 (1997).
9. H. He, M. E. J. Friese, N. R. Heckenberg, and H. Rubinsztein-Dunlop, Phys. Rev. Lett. **75**, 826 (1995).
10. K. Dholakia and T. Cizmar, Nat. Photonics **5**, 335 (2011).
11. J. Wang, J. Y. Yang, I. M. Fazal, N. Ahmed, Y. Yan, H. Huang, Y. Ren, Y. Yue, S. Dolinar, M. Tur, and A. E. Willner, Nat. Photonics **6**, 488 (2012).
12. A. Mair, A. Vaziri, G. Weihs, and A. Zeilinger, Nature **412**, 313 (2001).
13. R. Fickler, R. Lapkiewicz, W. N. Plick, M. Krenn, C. Schaeff, S. Ramelow, and A. Zeilinger, Science **338**, 640 (2012).
14. K. Dholakia, N. B. Simpson, M. J. Padgett, and L. Allen, Phys. Rev. A **54**, R3742 (1996).
15. N. Voloch-Bloch, K. Shemer, A. Shapira, R. Shiloh, I. Juwiler, and A. Arie, Phys. Rev. Lett. **108**, 233902 (2012).
16. A. Shapira, R. Shiloh, I. Juwiler, and A. Arie, Opt. Lett. **37**, 2136 (2012).
17. S. Franke-Arnold, S. M. Barnett, M. J. Padgett, and L. Allen, Phys. Rev. A **65**, 033823 (2002).
18. S. M. Saltiel, D. N. Neshev, W. Krolikowski, N. Voloch-Bloch, A. Arie, O. Bang, and Y. S. Kivshar, Phys. Rev. Lett. **104**, 083902 (2010).
19. F. A. Bovino, M. Braccini, M. Giardina, and C. Sibilia, J. Opt. Soc. Am. B **28**, 2806 (2011).
20. S. M. Saltiel, D. N. Neshev, W. Krolikowski, A. Arie, O. Bang, and Y. S. Kivshar, Opt. Lett. **34**, 848 (2009).
21. I. Dolev, A. Libster, and A. Arie, Appl. Phys. Lett. **101**, 101109 (2012).